New Journal of Physics
The open access journal for physics

Ultrahigh compression of water using intense heavy ion beams: laboratory planetary physics

N A Tahir[1,7], Th Stöhlker[1], A Shutov[2], I V Lomonosov[2], V E Fortov[2], M French[3], N Nettelmann[3], R Redmer[3], A R Piriz[4], C Deutsch[5], Y Zhao[6], P Zhang[6], H Xu[6], G Xiao[6] and W Zhan[6]

[1] GSI Helmholzzentrun für Schwerionenforschung, 64291 Darmstadt, Germany
[2] Institute of Problems of Chemical Physics, Russian Academy of Sciences, Institutskii pr. 18, 142432 Chernogolovka, Russia
[3] Institute of Physics, Universität Rostock, 18051 Rostock, Germany
[4] E.T.S.I. Industriales, Universidad de Castilla-La Mancha, 13071 Ciudad Real, Spain
[5] Laboratoire de Physique des Gaz et des Plasmas, Universite Paris-Sud, 91405 Orsay, France
[6] Institute of Modern Physics, Chinese Academy of Science, 730000 Lanzhou, People's Republic of China
E-mail: n.tahir@gsi.de

New Journal of Physics **12** (2010) 073022 (17pp)
Received 4 May 2010
Published 22 July 2010
Online at http://www.njp.org/
doi:10.1088/1367-2630/12/7/073022

Abstract. Intense heavy ion beams offer a unique tool for generating samples of high energy density matter with extreme conditions of density and pressure that are believed to exist in the interiors of giant planets. An international accelerator facility named FAIR (Facility for Antiprotons and Ion Research) is being constructed at Darmstadt, which will be completed around the year 2015. It is expected that this accelerator facility will deliver a bunched uranium beam with an intensity of 5×10^{11} ions per spill with a bunch length of 50–100 ns. An experiment named LAPLAS (Laboratory Planetary Sciences) has been proposed to achieve a low-entropy compression of a sample material like hydrogen or water (which are believed to be abundant in giant planets) that is imploded in a multi-layered target by the ion beam. Detailed numerical simulations have shown that using parameters of the heavy ion beam that will be available at FAIR, one can generate physical conditions that have been predicted to exist in the interior of giant planets. In the present paper, we report simulations of compression of

[7] Author to whom any correspondence should be addressed.

water that show that one can generate a plasma phase as well as a superionic phase of water in the LAPLAS experiments.

Contents

1. Introduction **2**
2. The Laboratory Planetary Sciences (LAPLAS) experimental scheme **4**
2.1. LAPLAS using an annular focal spot 4
2.2. LAPLAS using a circular focal spot 5
3. The choice of target material and its implications for hydrodynamic stability **5**
4. The *ab initio* equation of state (EOS) of water **7**
5. The Facility for Antiprotons and Ion Research (FAIR) beam parameters **8**
6. Simulation results **9**
6.1. Using an annular focal spot 9
6.2. Using a circular focal spot 11
7. Summary and conclusion **14**
Acknowledgments **15**
References **15**

1. Introduction

The interior of planets consists of matter under extreme conditions. For instance, at the center of Jupiter, which is the biggest planet in our solar system, temperatures of about 20 000 K and pressures of about 40 Mbar occur [1]–[7]. Besides Jupiter, other giant planets in our solar system (Saturn, Uranus and Neptune) and also planets detected around other stars are the subject of intense research—almost 400 extrasolar planet candidates are known today [8].

Matter in giant planets exists at high energy density (HED) so that correlations and quantum effects become increasingly important. Therefore, a reasonable description of planetary interiors, their structure and evolution is simultaneously also a great challenge to methods of many-body theory. Accurate equation of state (EOS) data for the most abundant elements represent the most important input into models of planetary interiors. The high-pressure phase diagram and the location of the melting line are also of great interest in this context. Furthermore, non-metal-to-metal transitions occur at high pressures, e.g. in hydrogen, which could possibly be accompanied by first-order phase transitions such as the plasma phase transition that has been predicted for decades [9], or a liquid–liquid transition. Other high-pressure effects such as demixing of hydrogen and helium [10, 11] or the existence of a superionic water phase [12]–[16] are also of great importance.

The generation and diagnostics of such extreme states of matter in the laboratory require novel experimental techniques. Today static compression experiments can access the light elements of interest—in this context, hydrogen and helium but also carbon, nitrogen and oxygen as well as their hydrogen compounds methane, ammonia and water—up to several Mbar but only at relatively low temperatures [17, 18]. Dynamic methods use shock waves to generate high pressures of up to several Mbar and temperatures of up to several 10 000 K, as demonstrated successfully for hydrogen, helium and water. High explosives [19], gas guns [20, 21], lasers [22, 23] and pulsed power [24] have been used as drivers for these single or

multiple shock wave experiments. Thereby, enormous progress has been made in high-pressure physics, but states deep in the interior of giant planets at tens of Mbar are not accessible yet.

Over the past decade, substantial progress has been made in the technology of strongly bunched, well-focused, high-quality intense heavy ion beams. Theoretical work on beam–matter heating has shown that such intense beams have great potential for generating extreme states in matter in the parameter space that is not accessible with traditional methods [25]–[42]. An intense heavy ion beam is therefore a novel tool to study the field of HED physics (HEDP), including planetary interiors.

The above different HEDP drivers have their advantages and disadvantages, as briefly discussed below. When a laser beam is incident on a solid target, material ablates from the target surface due to strong heating and the ablating material generates an ablation pressure that drives a strong shock wave into the target. It is to be noted that only a fraction of the incident laser energy is absorbed by the target while the rest is lost due to reflection, thereby reducing the beam–target coupling efficiency. A higher laser intensity is desirable to achieve higher ablation pressure; however, the intensity is limited in order to avoid the generation of suprathermal electrons that could severely degrade the compression as a result of preheat. Moreover, because of the sharp gradients in density, temperature and pressure, the physical conditions may not be uniform in laser-generated HED matter samples.

Energetic ions, on the other hand, penetrate deep into solid matter and deposit their energy quasi-uniformly over extended volumes of the target, thereby generating large samples (mm^3 or even cm^3) of HED matter with fairly uniform physical conditions. The beam–target coupling efficiency is large and beam–target interaction does not lead to any preheat mechanism. Since the ion beam deposits energy directly into solid matter, even a moderate beam intensity will generate pressure in the multi-Mbar range (despite a relatively low induced temperature [27]) that will drive a strong shock into the target.

The energy released by high-power chemical explosives, gas guns and pulse power machines is used to accelerate solid plates (flyer) that impact on the target to drive a strong shock in the sample to generate HED matter.

The GSI Helmholzzentrum für Schwerionenforschung (GIS), Darmstadt has unique accelerator facilities capable of delivering intense particle beams of all stable species, from protons up to uranium. The accelerator capabilities of the GSI will be improved tremendously after the completion of a new international accelerator project, FAIR (Facility for Antiprotons and Ion Research) [43], which has already entered the construction phase. An extensive experimental program for HED physics research, named **HEDgeHOB** (**H**igh **E**nergy **D**ensity Matter **Ge**nerated by **H**eavy I**o**n **B**eams), has been worked out for the FAIR accelerator. One of the important experiments to be conducted within the framework of this program is named **LAPLAS** (**LA**boratory **PLA**netary **S**cience), in which a low-entropy compression scheme will be used to generate physical conditions that are expected to exist in the interiors of giant planets. Previously [28, 30], [33]–[35], [37], [40]–[42], we simulated the compression of hydrogen in a LAPLAS scheme and this work showed that one can generate ultrahigh pressures of the order of 30 Mbar and ultrahigh densities of up to $3\,g\,cm^{-3}$ (30 times solid hydrogen density) using such a scheme. In the present study we report calculations on the compression of water, which is another important material that is presumably abundant in giant planets.

In section 2 we describe the LAPLAS scheme and in section 3 we discuss the influence of material properties on the hydrodynamic stability of the implosion. Section 4 summarizes the model of an *ab initio* EOS of water based on quantum molecular dynamics (QMD) that

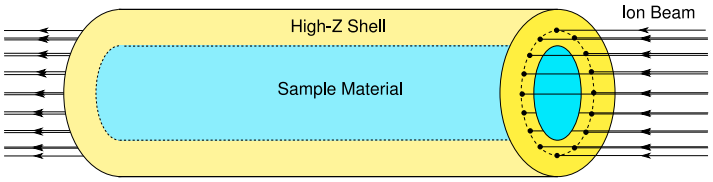

Figure 1. Beam–target setup of the LAPLAS scheme using an annular focal spot.

has been used in these calculations, whereas section 5 gives the FAIR beam parameters. The simulation results are presented in section 6 while the conclusions drawn from this work are noted in section 7.

2. The Laboratory Planetary Sciences (LAPLAS) experimental scheme

This experimental scheme proposes a low-entropy compression of a material such as frozen hydrogen or ice (water) that is enclosed in a cylindrical shell of a high-Z material. This type of experiment is suitable for studying the problem of hydrogen metallization [17, 18, 22, 23, 44] as well as for generating physical conditions that are expected to exist in the interiors of giant planets [1]–[7]. There are two proposed beam–target configurations for this experimental setup. In one case a hollow beam with an annular focal spot is used to drive the target, while in the other case a simple beam with a circular focal spot having a Gaussian transverse intensity distribution is employed. These two cases are described in the following subsections.

2.1. LAPLAS using an annular focal spot

The proposed beam–target geometry is shown in figure 1. The target consists of a cylinder of frozen sample material (for example, hydrogen or water) that is surrounded by a thick shell of a heavy material. One face of the target is irradiated with an intense heavy ion beam that has an annular (ring-shaped) focal spot. We assume that the inner radius of the annulus is larger than the radius of the sample material, which is a necessary condition to avoid direct heating of the sample by the ion beam (see figure 2). Moreover, we consider that the outer radius of the focal spot ring is smaller than the outer radius of the surrounding shell. It is seen from figure 2 that a layer of cold material from the outer shell known as ‘pusher’ or ‘payload’ is created between the sample material and the beam-heated region. The payload plays an important role in placing the compression on the desired adiabat. It is also seen that a cold shell around the beam-heated zone remains as a tamper that confines the implosion for a longer time.

The target length is assumed to be less than the range of the driver ions so that the energy deposition in the longitudinal direction is uniform. The pressure in the beam-heated region increases substantially and launches a shock wave inwards, along the radial direction. The shock wave enters the pusher, is subsequently transmitted into the sample and is then reflected at the cylinder axis. The reflected shock wave moves outwards along the radial direction and is again re-reflected at the sample–shell boundary. The boundary continues to move inwards, thereby compressing the sample slowly. This scheme generates a low-entropy compression of the sample material that leads to ultrahigh densities, ultrahigh pressures, but relatively low temperatures. This scheme is suited to explore the parameter domain relevant for hydrogen metallization [17, 18, 20, 22, 23, 44] as well as for planetary interiors [1]–[7].

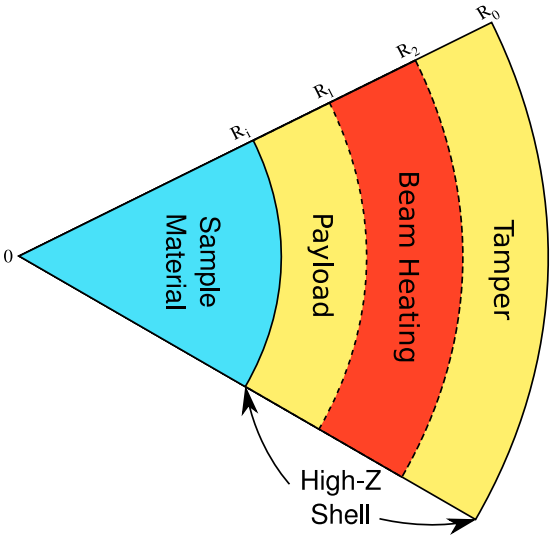

Figure 2. Cross-sectional view of the target shown in figure 1.

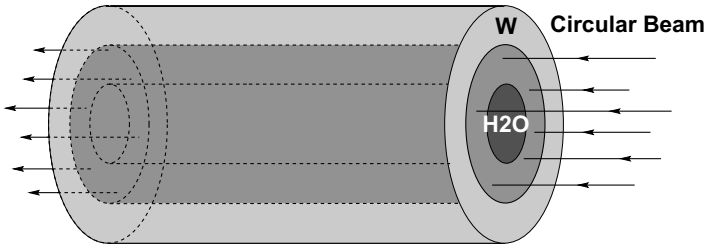

Figure 3. Beam–target setup of the LAPLAS scheme using a circular focal spot.

We note that the generation of an annular focal spot is a challenging problem. It has been previously demonstrated that a ring-shaped focal spot can be generated using a plasma lens [45]. An alternative approach has recently been suggested to employ an rf-wobbler that will rotate the beam with a very high frequency (of the order of a GHz) that will generate the required focal spot geometry. A detailed analysis of the symmetry issues of energy deposition in the target using such a system has been worked out in detail and the results have been published elsewhere [38, 39].

2.2. LAPLAS using a circular focal spot

Figure 3 shows the case where one uses a circular focal spot instead of an annular focal spot. In this case the sample is also directly heated by the beam, but since the pressure in the surrounding high-density shell is significantly higher than in the sample, the sample is still compressed to very high densities. However, the final temperature, in this case, is much higher (of the order of a few eV) than that in the previous one.

3. The choice of target material and its implications for hydrodynamic stability

One issue of possible concern in the design of the LAPLAS experiments is the onset of Rayleigh–Taylor instability (RTI) during the implosion process. In fact, an rf-wobbler will be used to rotate the beam in order to generate a ring-shaped focal spot that will heat the

annular region (the absorber) surrounding a pusher made of a heavy metal. This wobbler system will generate an azimuthal asymmetry [38, 39] that can seed hydrodynamic instabilities at the absorber/pusher interface that may spoil the performance of the implosion. Since the pusher remains in solid state during the implosion, the RTI will be controlled by the mechanical properties of the pusher material. Therefore, RTI is of central importance in the design of this experiment as well as in several other experiments on HED physics. However, in contrast to the classical case involving Newtonian or ideal fluids [46, 47], RTI in accelerated solids has been poorly understood so far, although it has been a subject of research for more than forty years [46]–[62]. The difficulties of constructing a compelling theory of the linear growth phase of RTI in solids have been essentially due to the character of the elastic–plastic constitutive properties of a solid, which have a nonlinear dependence on the magnitude of the rate of deformation.

We have recently developed a relatively simple, nevertheless accurate, model of the RTI in elastic–plastic solids [63, 64], and we have come up with a stability criterion that shows that transition to a plastic regime is a necessary but not a sufficient condition for instability as was erroneously assumed in [60]–[62]. Let us briefly review the essential features of this model.

For constructing the model, we have assumed a uniform plate of density ρ that is thick enough ($kh \gg 1$) so that finite thickness effects can be neglected. The plate is in the plane (x, z) and has been accelerated for a very long time until $t = 0$ by a constant and uniform pressure p_0 that represents a low-density fluid accelerating the plate with an acceleration $\vec{a} = -g\vec{e}_y$ ($g = p_0/\rho h$). At $t = 0$, a ripple $\delta p = p_0(\xi_0/h)\sin kx$ is superposed on the uniform pressure p_0. With the previous considerations the linear evolution of the perturbation amplitude can be well described by the following equation of motion [40], [63]–[66]:

$$\frac{\rho}{k}\ddot{\eta} = \rho g(\eta + \eta_0) - S_{yy}, \tag{1}$$

where $\eta(x, y, t) = \xi(t)\mathrm{e}^{ky}\sin kx$ because we assume that the perturbed velocity field can be approximated by one corresponding to an inviscid ideal fluid. $\xi(t)$ is the instantaneous perturbation amplitude on the interface and S_{yy} represents the force per unit area due to the mechanical properties of the medium. S_{yy} is given by the normal component of the deviatoric part of the stress tensor $\sigma_{ij} = -p\delta_{ij} + S_{ij}$ (p is the thermodynamic pressure and δ_{ij} is the Kronecker tensor) and it can be obtained from the Prandtl–Reuss equations: $S_{yy} = 2kG\eta$ for $\eta \leqslant \eta_\mathrm{p}$, and $S_{yy} = Y/\sqrt{3}\,\sin kx$ for $\eta \geqslant \eta_\mathrm{p}$, where η_p is the value of η for which the elastic limit is achieved. G and Y are the shear modulus and the yield strength of the solid, respectively. Since the onset of plastic flow occurs first on the interface and then progresses towards the plate interior, its effects on the instability are not felt until it has affected a region with thickness of the order of k^{-1}. Therefore, by evaluating equation (1) at $y = y_\mathrm{p} \approx -k^{-1}$ we obtain $\ddot{\xi} = kg(\xi + \xi_0) - 2k^2G\xi/\rho$ for $\xi \leqslant \xi_\mathrm{p}$, and $\ddot{\xi} = kg(\xi + \xi_0) - \alpha Yk/\rho\sqrt{3}$ for $\xi \geqslant \xi_\mathrm{p}$ ($\xi_\mathrm{p} = \alpha Y/2\sqrt{3}kG$). Since $\alpha = \mathrm{e}^{k|y_\mathrm{p}|}$, we take $\alpha = 3$. In addition, since we choose to perturb the driving pressure, $\xi(0) = 0$.

From the previous equation of motion for the interface, we can obtain the condition for marginal stability determining the instability threshold [63, 64]:

$$(\rho g\xi_0/\sqrt{3}Y)_\mathrm{TH} = 1 - \sqrt{\rho g\lambda/4\pi G}. \tag{2}$$

We can also obtain the condition for the elastic to plastic transition (EP transition) by requiring that the maximum amplitude z_m^e be equal to the amplitude $z_\mathrm{p} = \hat{\lambda}/\hat{\xi}$, which is necessary to reach

Table 1. Material data from [69].

Material	Y (GPa)	G (GPa)	ρ (g cm^{-3})	T_{melting} (K)	Vote
W	2.2–4.0	160	19.25	4520	Very good
Ta	0.77–1.0	70	16.65	4340	Very good
Nb	0.70–1.4	85.5	8.57	2330	Quite good
Ti	0.71–1.45	43.4	4.51	2260	Quite good
Steel	0.34–2.5	77	7.85	2380	Good
Be	0.33–1.23	151	1.85	1820	Good
Al	0.29–0.68	27.6	52.7	1220	Not bad
Au	0.02–0.225	28	19.3	1970	Bad
Pb	0.008–0.1	8.6	11.34	760	Very bad

the elastic limit [63, 64]:

$$(\rho g \xi_0/\sqrt{3}Y)_{\text{EP}} = (1 - \rho g \lambda/4\pi G)/2. \tag{3}$$

Equations (2) and (3) determine the boundaries for the existence of stability after the elastic limit has been reached.

These results have direct implications on the design of experiments on HED physics. For the particular case of the LAPLAS experiments, equation (2) helps to make the best choice for the pusher material in the cylindrical shell target. In fact, to ensure stabilizing effects from the constitutive properties of the pusher material, we require, at least, that $Y > (p_0/\sqrt{3})(\xi_0/h)$. In the LAPLAS experiments the asymmetry level will be essentially determined by the wobbler system producing the beam rotation for heating the annular absorber region. For a typical parabolic power pulse, the asymmetry level ξ_0/h has been shown to be $= 1/N^2$, where N is the number of revolutions of the beam during the pulse duration τ_{beam} [37, 38]. At present, FAIR is designed to deliver pulses with $\tau_{\text{beam}} \approx 100$ ns and the wobbler system is being designed to generate more than 30 revolutions during this pulse duration [67]. Thus, $\xi_0/h \approx 10^{-3}$. For driving pressures in the range of 1–10 Mbar, we need $Y > 0.06$–0.6 GPa. The materials considered so far for LAPLAS have been gold and lead because of their high densities ($\rho_{\text{Au}} = 19.3$ g cm^{-3}; $\rho_{\text{Pb}} = 11.3$ g cm^{-3}). According to [68] the maximum values of Y reported in the literature for gold and lead are, respectively, 0.225 and 0.1 GPa, which may make them not very suitable materials for LAPLAS targets from the point of view of implosion stability (see table 1). Better choices would be tungsten and tantalum, which have similar densities ($\rho_{\text{W}} = 19.3$ g cm^{-3} and $\rho_{\text{Ta}} = 16.7$ g cm^{-3}) but higher values of Y ($Y_{\text{W}} = 2.2$–4 GPa and $Y_{\text{Ta}} = 0.77$–1 GPa), besides having the highest melting temperatures and high values of G ($G_{\text{W}} = 160$ GPa and $G_{\text{Ta}} = 69$ GPa).

4. The *ab initio* equation of state (EOS) of water

The *ab initio* EOS of water [16] was obtained by QMD simulations. This method treats the electron system with finite-temperature density functional theory [69]–[71], which yields the forces that propagate protons and oxygen nuclei via a classical MD algorithm. The pressure, internal energy, and structural and transport properties are obtained as time averages once

Table 2. Comparison between existing and future beam parameters.

	SIS18	SIS100
Intensity (ions per bunch)	4×10^9	5×10^{11}
Bunch length (ns)	130	50
Particle energy (MeV u^{-1})	400	400–2700
Specific energy deposition (kJ g^{-1})	1.0	125
Specific power deposition (TW g^{-1})	0.005	2.5

thermodynamic equilibrium has been reached. The *ab initio* EOS data are converged to a general accuracy of 1–2% and the pressures are in good agreement with diamond anvil cell data. The *ab initio* pressure increases significantly stronger with density than with pressure from the widely used SESAME 7150 table [72]. As the temperature rises to several 1000 K, the water molecules dissociate and ionize to form a dense plasma. At high densities, the QMD simulations also predict a superionic phase [12] with strongly diffusive protons but immobile oxygen ions that occupy bcc lattice positions. The superionic phase shows high proton conductivity but suppressed electronic conductivity compared with the plasma phase [15].

5. The Facility for Antiprotons and Ion Research (FAIR) beam parameters

A new powerful heavy ion synchrotron, SIS100 (100 Tm magnetic rigidity), will be built within the framework of FAIR at Darmstadt, which will deliver an intense beam of heaviest particles (uranium) with unprecedented intensities. According to optimum design parameters, the beam intensity will be $N = 5 \times 10^{11}$ ions that will be delivered in a single bunch, 50–100 ns long. A wide range of particle energy, namely 400–2700 MeV u^{-1}, will be available, which will provide great flexibility to experiment designers. The transverse beam intensity will be Gaussian and, for HEDP experiments, the beam will be focused to a very small focal spot size with a full width at half maximum (FWHM) of about 1 mm. For the LAPLAS experiments, a wobbler is being designed that will generate an annular focal spot.

Table 2 shows the comparison between currently available beam parameters at the existing GSI heavy ion synchrotron, SIS18 and at the future SIS100 accelerator. It is seen that when SIS100 works at full capacity, beam intensity increases by a factor of 100 while specific energy deposition and specific power deposition in the target material increase to unprecedented levels.

It is also to be noted that plans are being made to construct a huge accelerator facility at the Institute of Modern Physics, Lanzou, China, with the aim of generating an intense uranium beam. It is expected that in phase I, a $^{238}U^{4+}$ beam with a particle energy of 1.29 GeV u^{-1} and an intensity of 10^{12} ions per bunch will be accelerated. In phase II, a higher particle energy of 3.2 GeV u^{-1} and an intensity of 10^{13} ions per bunch will be achieved [73]. It has been proposed that the construction of this facility may start in the year 2020, which will be a big step forward in accelerator technology. The expected beam parameters will provide a unique opportunity to perform novel experiments in HEDP. It is also to be noted that the beam intensity required to implode reactor-size inertial fusion targets [78]–[88] is about 10^{15} ions per bunch and one requires a bunch length of the order of 10 ns. Nevertheless, one will be able to carry out implosion experiments on a smaller scale; especially, it will be possible to study the target physics in the prepulse regime.

6. Simulation results

In this section, we report numerical simulation results employing the two LAPLAS implosion schemes using water as the sample material. As discussed in section 3, lead and gold are not favorable materials due to their low values of yield strength. In the present study, we therefore use tungsten to construct the outer high-Z shell. The simulations were carried out using a two-dimensional hydrodynamic computer code, BIG2 [74], which is based on a Godunov-type scheme. For tungsten we use a semi-empirical EOS [75, 76], whereas for water we use the EOS described in section 4 and [16]. The ion energy loss in the target is calculated using the SRIM code [77], which is based on the cold stopping model. This is a reasonable approximation because the target temperature is not very high and the ionization effects on the stopping can be neglected.

6.1. Using an annular focal spot

The target length is $L = 7$ mm, the radius of the sample (water) layer $R_i = 0.2$ mm and the outer target radius $R_o = 3$ mm. The ion energy is considered to be 1.5 GeV u^{-1} and the bunch length is 50 ns. The inner radius of the annular ring is $R_1 = 0.4$ mm and the outer radius is $R_2 = 1.4$ mm. We have considered different values of the beam intensity, N, including 10^{11}, 3×10^{11} and 5×10^{11} ions per bunch, respectively.

The range of the 1.5 GeV u^{-1} uranium ions is significantly larger than the length of the cylinder, and therefore the Bragg peak lies outside the target that leads to fairly uniform energy deposition along the particle trajectory. We have considered tungsten as the outer shell material, and the results are presented in the following.

In figure 4(a) we present the specific energy deposition in the target in the r–Z plane at $t = 50$ ns, a time when the beam has just delivered its total energy. The beam is incident at the right side of the target and the particles penetrate through the cylinder, thereby depositing energy uniformly along their trajectories. It is seen that the specific energy deposition at the maxima of the Gaussian distribution in the tungsten shell is about 20 kJ g^{-1}. The corresponding temperature distribution is presented in figure 4(b), which shows a maximum temperature of the order of 10^5 K. The pressure distribution generated in the target is shown in figure 4(c), which shows a maximum pressure of 3.7 Mbar. The high pressure in the tungsten shell generates an outgoing as well as an inmoving shock, which are clearly seen in figure 4(d), where the density distribution is presented. The payload density has been increased to about 25 g cm^{-3} due to the compression by the inmoving shock, which is subsequently transmitted into the water region and reverberates between the cylinder axis and the water–tungsten boundary.

In figure 5(a) we present the density distribution at $t = 100$ ns. It is seen that the inner target radius has already been reduced, which means compression of the water. The process of multiple shock reflection is seen in figure 5(b), where we plot the density versus radius at $L = 3.5$ mm in the water region at different times. This multiple shock reflection scheme leads to a low-entropy compression of the sample material. The compression results are shown in figures 6(a)–(c), where we plot the density, temperature and pressure versus radius at $L = 3.5$ mm in water at the time of maximum compression using different values of N, namely 5×10^{11}, 3×10^{11} and 10^{11} ions per bunch, respectively. It is seen in figure 6(a) that the radius of the water region has been reduced to 75 μm from an initial value of 200 μm. The water density is about 7 g cm^{-3} while the temperature within the inner 20 μm is high, which corresponds to a plasma state. In

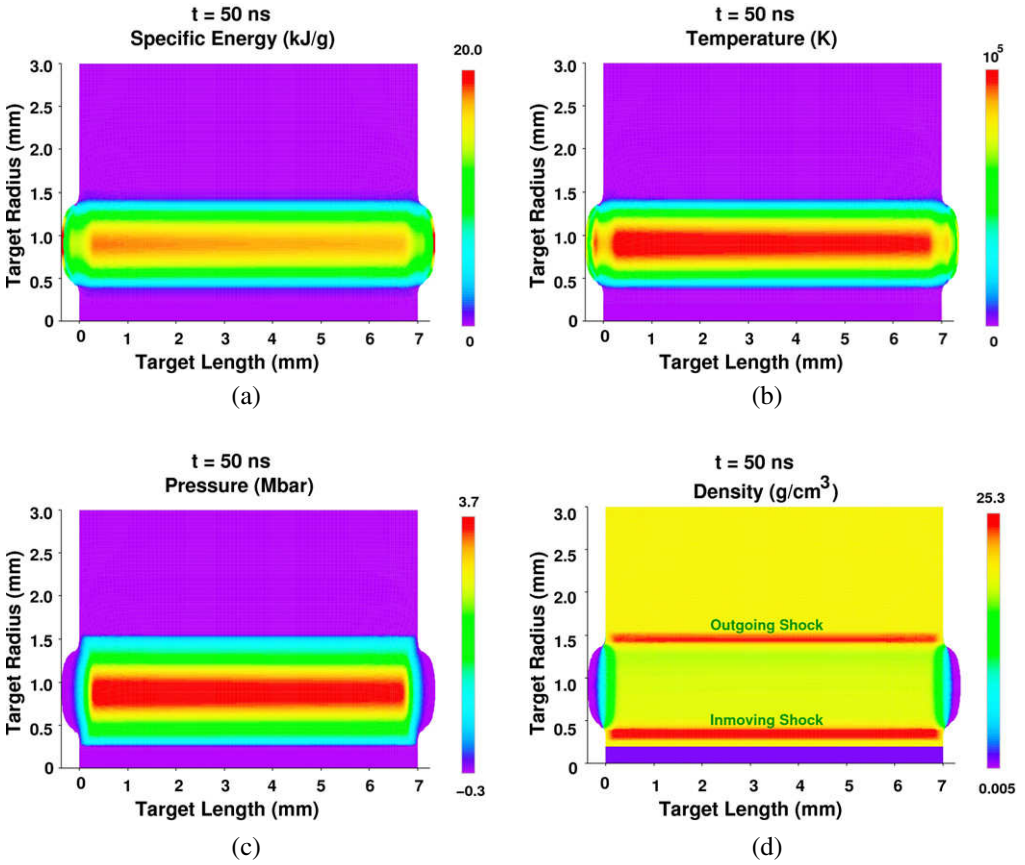

Figure 4. Cylindrical multi-layered target (water enclosed in tungsten shell), $L = 7$ mm, $R_i = 0.2$ mm, $R_o = 3.0$ mm facially irradiated by a uranium beam, particle energy 1.5 GeV u^{-1}, $N = 5 \times 10^{11}$ ions per bunch, bunch length = 50 ns, annular focal spot with $R_1 = 0.4$ mm, $R_2 = 1.4$ mm: (a) specific energy deposition; (b) temperature; (c) pressure; and (d) density; in the r–Z plane at $t = 50$ ns.

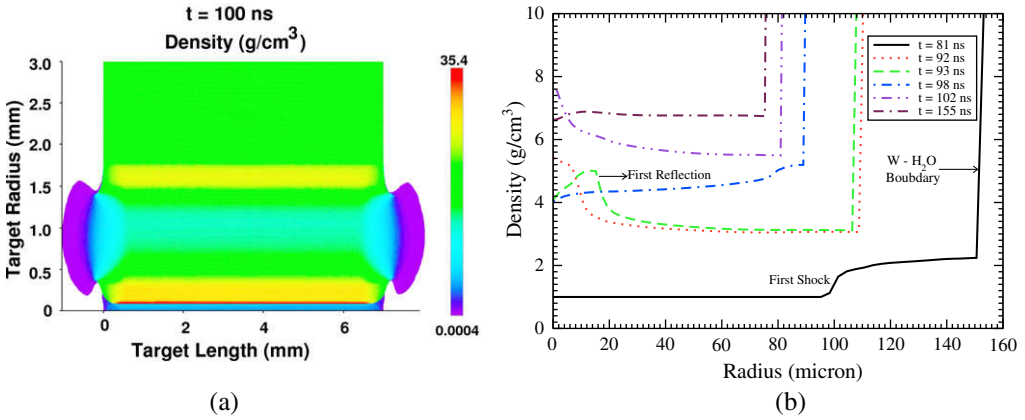

Figure 5. (a) Density at $t = 100$ ns corresponding to the case presented in figure 4; (b) density versus radius at $L = 3.5$ mm at different times.

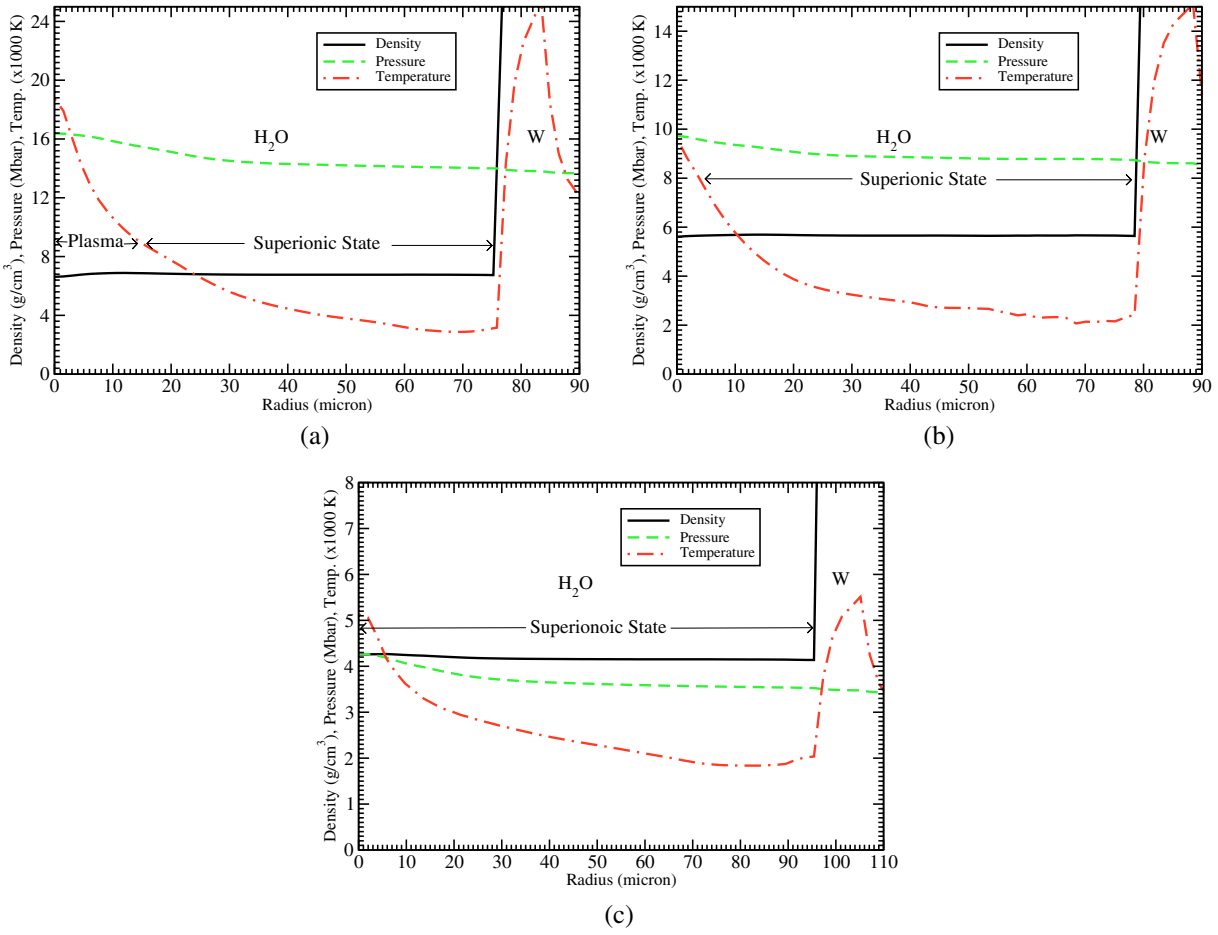

Figure 6. Density, temperature and pressure versus target radius at $L = 3.5$ mm in water at the time of maximum compression: (a) $N = 5 \times 10^{11}$, (b) $N = 3 \times 10^{11}$ and (c) $N = 10^{11}$ using a tungsten outer shell driven by an annular focal spot.

the outer part, however, the temperature is below 7000 K and the pressure is of the order of 15 Mbar, which corresponds to a superionic state of water in which the protons are mobile in an oxygen lattice [16]. The following figures show that as the beam intensity decreases, the density, temperature and pressure in the compressed water decrease and the region in which the superionic phase exists increases. Figure 6(c) shows that in the case of $N = 10^{11}$ ions per bunch, the maximum density is 4.5 g cm^{-3}, the maximum pressure is about 4 Mbar and the average temperature is of the order of 3000 K, and the entire sample is in a superionic phase.

This is an important result because the beam intensity at FAIR will increase gradually before achieving the maximum value. Therefore, one will be able to carry out very interesting experiments even with significantly lower beam intensities that will be available during the initial stages of the FAIR project.

6.2. Using a circular focal spot

Since construction of the wobbler system is a challenging problem, we also worked on an alternative LAPLAS scheme in case the availability of the wobbler is delayed. In this alternative

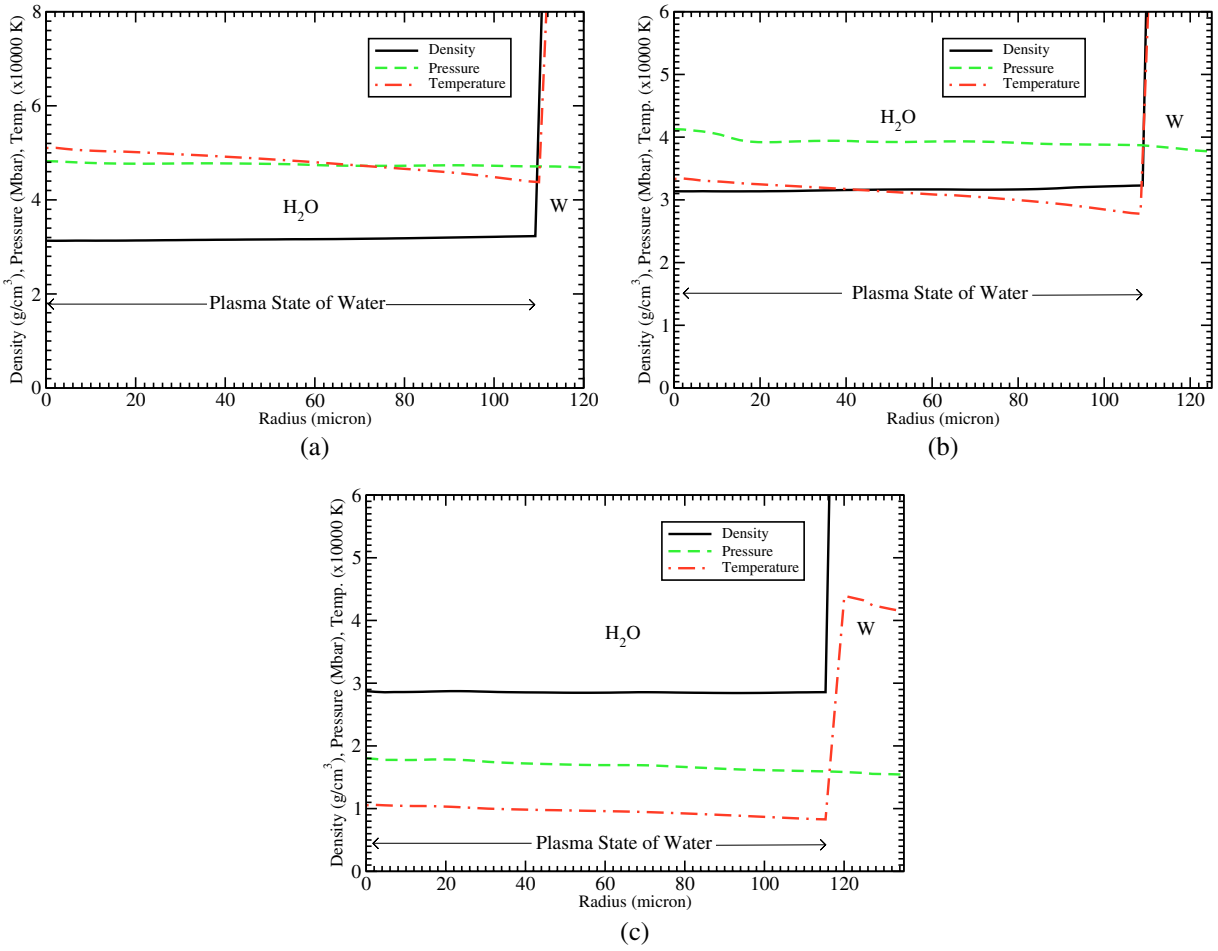

Figure 7. Density, temperature and pressure versus target radius at $L = 3.5$ mm in water at the time of maximum compression: (a) $N = 5 \times 10^{11}$, (b) $N = 3 \times 10^{11}$ and (c) $N = 10^{11}$ using a tungsten outer shell driven by a circular focal spot with FWHM = 1.5 mm.

scheme, a circular focal spot with a Gaussian transverse intensity distribution is used that facially irradiates the LAPLAS target (see figure 3). In such a beam–target configuration, the sample material is also strongly heated by the ion beam together with a part of the surrounding shell. However, due to the large density difference between the sample and the shell material, the pressure generated in the heated part of the shell is substantially higher than that in the sample. Therefore, the sample still gets highly compressed, although in this case the temperature is much higher than in the other case.

We have simulated three different cases that use different values of the beam intensity, $N = 5 \times 10^{11}$, 3×10^{11} and 10^{11} ions per bunch, respectively. A circular focal spot having a Gaussian transverse intensity distribution, with FWHM = 1.5 mm, is considered.

Figures 7(a)–(c) plot the density, temperature and pressure versus radius in water at the time of maximum compression using the above different values of the beam intensity. The outer shell of the target is made of tungsten. It is seen in figure 7(a) that for $N = 5 \times 10^{11}$ ions per bunch, one achieves a density of the order of 3 g cm^{-3} and a temperature of about 50 000 K

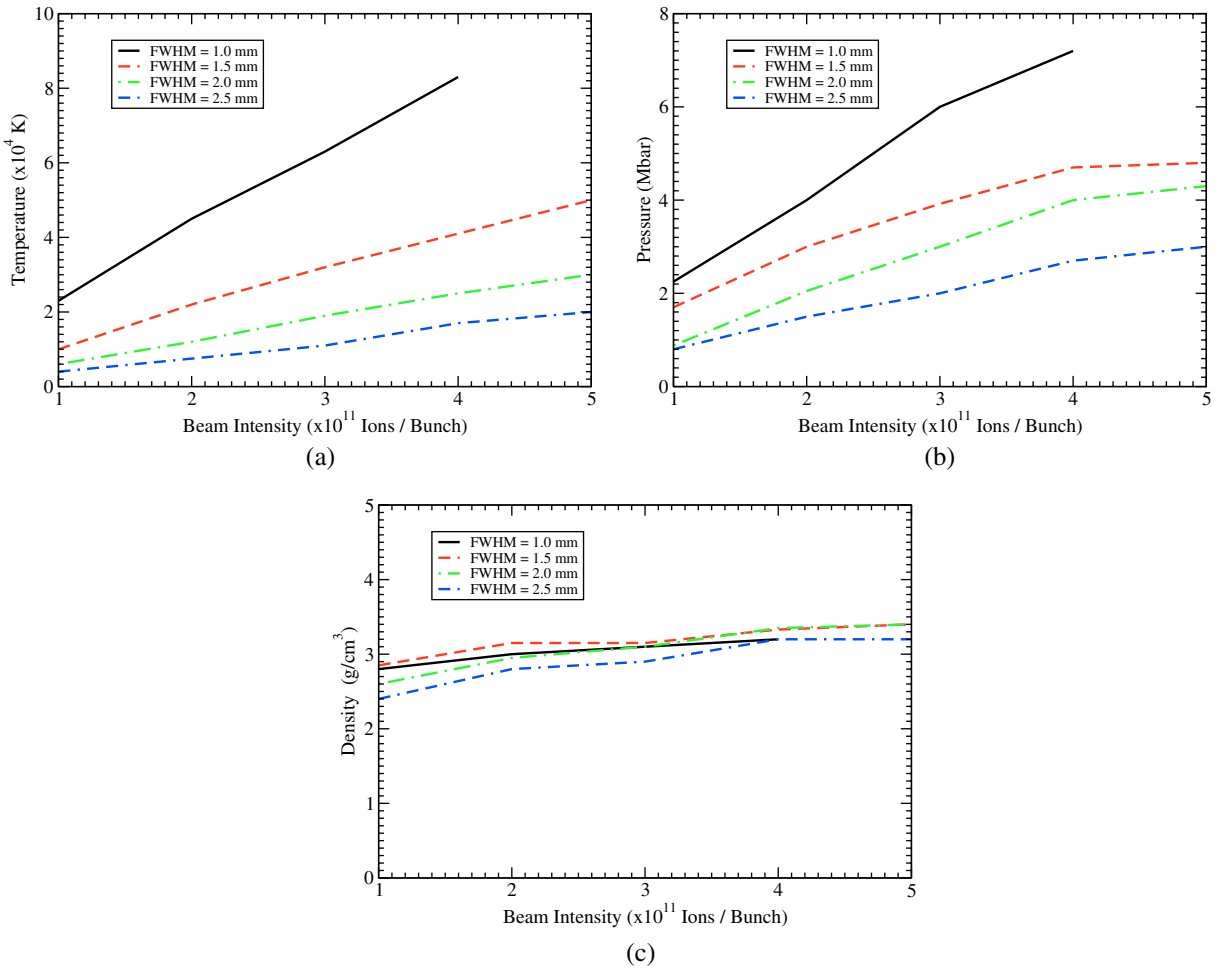

Figure 8. (a) Temperature versus N, (b) pressure versus N and (c) density versus N for a circular focal spot for different values of FWHM using a tungsten outer shell.

while the pressure is about 5 Mbar, which shows that one has a plasma phase of water in the entire sample. It is also worth noting that the temperature in this case is fairly uniform along the radius.

Figures 7(b) and (c) show that in all the different cases, one achieves the same material density, but the temperature is very different. In figure 7(c), which corresponds to a beam intensity of 10^{11} ions per bunch, the temperature is about 10 000 K. However, according to [16], the physical conditions achieved in all three different cases presented in figure 7 correspond to a plasma state of water. It is therefore concluded that using a LAPLAS scheme with a circular focal spot, one cannot achieve the superionic water phase. For this purpose, the availability of a wobbler system is absolutely essential.

In order to study the effect of focal spot size on compression, we also carried out simulations using different values of the focal spot size with FWHM = 1.0, 1.5, 2.0 and 2.5 mm, respectively, for different values of the beam intensity. The results are presented in figure 8. In figure 8(a) we plot the sample temperature versus beam intensity for the four different values of the FWHM. It is seen that using FWHM = 1.0 mm, the temperature increases from 20 000

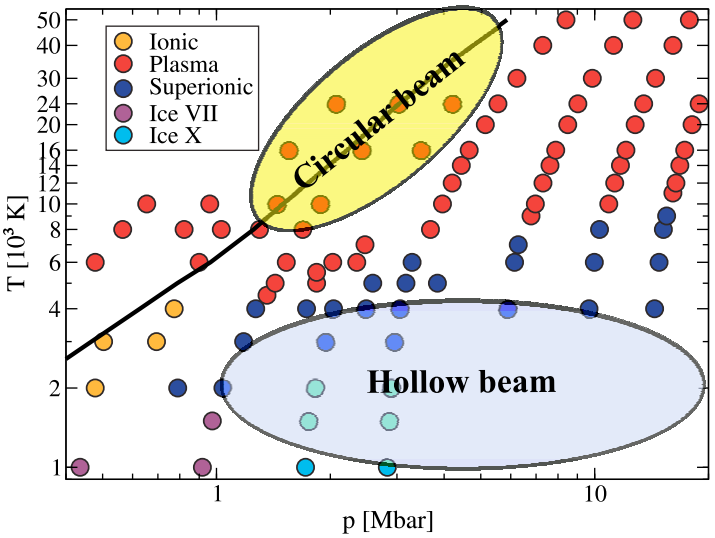

Figure 9. Each colored point corresponds to a QMD simulation in thermodynamic equilibrium. When the electronic conductivity exceeds 100 $(\text{ohm cm})^{-1}$ [15], the ionic (dissociated) fluid is labeled as plasma. The solid line is the principal Hugoniot curve.

to 80 000 K over the considered range of beam intensity. As the size of the focal spot increases, the specific energy deposition decreases (inversely proportional to the square of the spot radius) and, consequently, the temperature decreases.

The corresponding pressure profiles are presented in figure 8(b), which show behavior similar to the temperature profiles. It is seen that one can achieve a maximum pressure on the order of 7 Mbar using this scheme.

The density curves are presented in figure 8(c), which show that the final density is of the order of 3 g cm^{-3}. These figures again demonstrate that one can only access a plasma state of water using this scheme.

In figure 9 we present a phase diagram of water [16] in which the areas accessible in the LAPLAS experiments are highlighted. It is clearly seen that using a circular focal spot one can access the plasma state, whereas using an annular focal spot it is possible to generate the interesting superionic phase of water as well as Ice VII and Ice X phases.

7. Summary and conclusion

The FAIR accelerator facilities will provide very powerful high-quality heavy ion beams with unprecedented intensities. Extensive theoretical work on beam matter heating over the past decade [25]–[41] has shown that the ion beams that will be generated at FAIR will be a very unique and very efficient tool to study HEDP in those regions of parameter space that are not so easy to access with traditional methods. A detailed experimental program for HEDP studies, HEDgeHOB, has already been proposed. One of the experiments suggested in this proposal, LAPLAS, employs an ion beam to drive a low-entropy compression of a sample material like hydrogen or water that is enclosed in a cylindrical shell of a heavy material. Two different beam–target configurations have been worked out for this scheme. In one scheme, the target

implosion is driven by a hollow beam with an annular focal spot, whereas in the other case, a normal circular focal spot with a Gaussian transverse intensity distribution in the radial direction is considered.

In the present paper we report detailed hydrodynamic simulations of the compression of water, which presumably is abundantly found in some of the giant planets such as Uranus and Neptune. These simulations have been carried out using a two-dimensional computer code, BIG2 [74], which is based on a Gudonov-type scheme. For water, we use an *ab initio* EOS that is based on QMD [16]. Although the maximum beam intensity, N, at the FAIR accelerator is expected to be 5×10^{11} uranium ions per bunch, we have also carried out simulations using much lower values of N. This is because the beam intensity will increase gradually, and it is important to know if one can perform interesting experiments during the early stages of the FAIR project before the maximum intensity will be achieved.

It is reported that the stability of the implosion is dependent on the material properties of the surrounding shell. A higher yield strength is desirable for achieving this purpose. Gold and lead, which have been previously used as target materials, are not good from this point of view. It has been concluded that tungsten and niobium, which have densities similar to gold and lead, respectively, are more favorable. In the present paper, we have therefore used tungsten to construct the outer shell.

The results presented in this paper have shown that one can achieve the very interesting superionic phase of water [16] using the LAPLAS scheme driven by an annular focal spot. One achieves a density in the range of 5–7 g cm^{-3}, a temperature of the order of 2000–5000 K and a pressure between 4 and 16 Mbar, using beam intensities N from 10^{11}–5×10^{11} ions per bunch.

With a circular focal spot, on the other hand, the temperature is too high and one can only access the plasma state of water. The simulations show that for the above range of parameters, one achieves density of the order of 3 g cm^{-3}, temperature in the range of 8000–80 000 K and pressure between 0.8 and 7 Mbar.

Acknowledgments

We thank the BMBF, DFG within SFB 652 and grant RE 882/11, HLRN via grant mvp-00001, RFBR grant No. 08-02-92882-NNIO-a, Russia, Ministerio de Ciencia Innovacion (ENE2009-09276) and Consejeria de Ciencia Tecnologia of Spain (PAI08-0152-7994) for providing the financial support for this work.

References

[1] Guillot T and Vannier M 2003 *EAS Publ. Ser.* **8** 25
[2] Guillot T 1999 *Science* **286** 72
[3] Guillot T 1999 *Planet Space Sci.* **47** 1183
[4] Chabrier G, Saumon D, Hubbard W B and Lunine J I 1992 *Astrophys. J.* **391** 817
[5] Hubbard W B and Marley M S 1989 *Icarus* **78** 102
[6] Zarkov V N and Trubitsyn V P 1978 *Physics of Planetary Interiors* ed W B Hubbard (Tucson, AZ: Pachart Press)
[7] Nettelmann N, Holst B, Kietzmann A, French M, Redmer R and Blaschke D 2008 *Astrophys. J.* **683** 1217
[8] www.exoplanets.eu

[9] Redmer R, Holst B and Hensel F (ed) 2010 *Metal–Nonmetal Transitions* (*Springer Series in Material Sciences* vol 132) (Berlin: Springer)
[10] Lorenzen W, Holst B and Redmer R 2009 *Phys. Rev. Lett.* **102** 115701
[11] Vorberger J, Tamblin I, Militzer B and Bonev S A 2007 *Phys. Rev.* B **75** 024206
[12] Cavazzoni C, Chiarotti G L, Scandolo S, Tossatti E, Bernasconi M and Parrinello M 1999 *Science* **283** 44
[13] Henry E *et al* 2001 *Laser Part. Beams* **19** 111
[14] Goldman N, Fried L E, Kuo I F W and Mundy C J 2005 *Phys. Rev. Lett.* **94** 217801
[15] Mattsson T R and Desjarlais M 2006 *Phys. Rev. Lett.* **97** 017801
[16] French M, Mattsson T R, Nettelmann N and Redmer R 2009 *Phys. Rev.* B **79** 054107
[17] Mao H and Hemley R J 1994 *Rev. Mod. Phys.* **66** 671
[18] Narayana C, Luo H, Orloff J and Rouff A L 1998 *Nature* **393** 45
[19] Mintsev V B and Fortov V E 2006 *J. Phys. A: Math. Gen.* **39** 4319
[20] Nellis W J 2006 *Rep. Prog. Phys.* **69** 1479
[21] Mitchell A C and Nellis W J 1981 *J. Appl. Phys.* **52** 3363
[22] Celliers P M, Collins G W, Da Silva L B, Gold D M, Cauble R, Wallace R J, Foord M E and Hammel B A 2000 *Phys. Rev. Lett.* **84** 5564
[23] Cauble R, Celliers P M, Collins G W, Da Silva L B, Gold D M, Foord M E, Budil K S, Wallace R J and Ng A 2000 *Astrophys. J. Suppl. Ser.* **127** 267
[24] Knudson M D *et al* 2004 *Phys. Rev.* B **69** 144209
[25] Tahir N A, Hoffmann D H H, Maruhn J A, Lutz K-J and Bock R 1998 *Phys. Plasmas* **12** 4426
[26] Tahir N A, Hoffmann D H H, Maruhn J A, Spiller P and Bock R 1999 *Phys. Rev.* E **60** 4715
[27] Tahir N A, Kozyreva A, Spiller P, Hoffmann D H H and Shutov A 2001 *Phys. Rev.* E **63** 036407
[28] Tahir N A *et al* 2001 *Phys. Rev.* E **63** 016402
[29] Tahir N A *et al* 2003 *Phys. Rev. Spec. Top. Beams Accel.* **6** 020101
[30] Tahir N A *et al* 2003 *Phys. Rev.* B **67** 184101
[31] Tahir N A *et al* 2004 *Laser Part. Beams* **22** 485
[32] Tahir N A *et al* 2005 *Phys. Rev. Lett.* **95** 035001
[33] Tahir N A *et al* 2007 *Nucl. Instrum. Methods* A **577** 238
[34] Tahir N A, Piriz A R, Wouchuk G, Shutov A, Lomonosov I V, Fortov V E, Deutsch C and Hoffmann D H H 2009 *Nucl. Instrum. Methods* A **606** 177
[35] Tahir N A, Piriz A R, Wouchuk G, Shutov A, Lomonosov I V, Deutsch C, Hoffmann D H H and Fortov V E 2009 *Astrophys. Space Sci.* **322** 179
[36] Tahir N A, Spiller P, Shutov A, Lomonosov I V, Piriz A R, Redmer R, Hoffmann D H H, Fortov V E, Deutsch C and Bock R M 2009 *IEEE Trans. Plasma Sci.* **37** 1267
[37] Piriz A R, Portugues R, Tahir N A and Hoffmann D H H 2002 *Phys. Rev.* E **66** 056403
[38] Piriz A R, Tahir N A, Hoffmann D H H and Temporal M 2003 *Phys. Rev.* E **67** 017501
[39] Piriz A R, Temporal M, Lopez Cella J J, Tahir N A and Hoffmann D H H 2003 *Plasma Phys. Control. Fusion* **45** 1733
[40] Piriz A R, Lopez Cela J J, Serna Moreno M C, Tahir N A and Hoffmann D H H 2006 *Laser Part. Beams* **24** 465
[41] Piriz A R, Lopez Cela J J, Cortazar O D, Tahir N A and Hoffmann D H H 2005 *Phys. Rev.* E **72** 056313
[42] Temporal M, Lopez Cela J J, Piriz A R, Grandjouan N, Tahir N A and Hoffmann D H H 2003 *Laser Part. Beams* **21** 609
[43] Henning W F 2004 *Nucl. Instrum. Methods* A **214** 211
[44] Wigner E and Huntigton H B 1935 *J. Chem. Phys.* **3** 764
[45] Neuner U *et al* 2000 *Phys. Rev. Lett.* **85** 4518
[46] Rayleigh L 1965 *Scientific Papers* vol 2 (New York: Dover)
[47] Taylor G I 1950 *Proc. R. Soc.* A **201** 192
[48] Miles J W 1966 *General Dynamics Report* No. GAMD-7335, AD 643161 (unpublished)

[49] White G N 1973 *Los Alamos National Laboratory Report* No. LA-5225-MS (unpublished)
[50] Barnes J F, Blewet P J, McQueen R G, Meyer K A and Venable D 1974 *J. Appl. Phys.* **45** 727
[51] Barnes J F, Janney D H, London R K, Meyer K A and Sharp D H 1980 *J. Appl. Phys.* **51** 4678
[52] Dienes J K 1978 *Phys. Fluids* **21** 736
[53] Swegle J W and Robinson A C 1989 *J. Appl. Phys.* **66** 2838
[54] Robinson A C and Swegle J W 1989 *J. Appl. Phys.* **66** 2859
[55] Drucker D C 1980 *Mechanics Today* vol 5 ed S Nemmat-Nasser (Oxford: Pergamon) p 3
[56] Drucker D C 1980 *Ing. Arch.* **49** 361
[57] Ruden E L and Bell D E 1997 *J. Appl. Phys.* **82** 163
[58] Dimonte G, Gore R and Schneider M 1998 *Phys. Rev. Lett.* **80** 1212
[59] Dimonte G 1999 *Phys. Plasmas* **6** 2009
[60] Nizovtzev P N and Raevskii P N 1991 *VANT Ser. Teor. Prikl. Fiz.* **3** 11
[61] Lebedev A I, Nizovtzev P N, Raevskii P N and Solovev V P 1996 *Phys.—Dokl.* **41** 328
[62] Bakhrakh S M *et al* 1997 *Lawrence Livermore National Laboratory Report* No. UCRL-CR-126710 (unpublished)
[63] Piriz A R, Lopez-Cela J J and Tahir N A 2009 *J. Appl. Phys.* **105** 116101
[64] Piriz A R, Lopez-Cela J J and Tahir N A 2009 *Phys. Rev.* E **80** 046305
[65] Piriz S A, Piriz A R and Tahir N A 2009 *Phys. Plasmas* **16** 082706
[66] Piriz A R, Cortazar O D, Lopez-Cela J J and Tahir N A 2006 *Am. J. Phys.* **74** 1095
[67] Golubev A 2009 private communication
[68] Steinberg D J, Cochran S G and Guinan M W 1980 *J. Appl. Phys.* **51** 1428
[69] Hohenberg P and Kohn W 1964 *Phys. Rev.* B **136** 864
[70] Kohn W and Sham L J 1965 *Phys. Rev.* A **140** 1133
[71] Mermin N D 1965 *Phys. Rev.* A **137** 1441
[72] Lyon P S and Johnson J D (ed) 1992 SESAME: Los Alamos National Laboratories Equation of State Database *Los Alamos Report* No. LA-UR-92-3407
[73] Zhao Y 2009 private communication
[74] Fortov V E *et al* 1996 *Nucl. Sci. Eng.* **123** 169
[75] Lomonosov I V 2007 *Laser Part. Beams* **25** 567
[76] Lomonosov I V and Tahir N A 2007 *Appl. Phys. Lett.* **92** 101905
[77] Ziegler J F, Biersack J P and Littmark U 1996 *The Stopping and Ranges of Ions in Solids* (New York: Pergamon)
[78] Bangerter R O, Mark J W K and Thiessen A R 1982 *Phys. Lett.* A **88** 225
[79] Tahir N A and Long K A 1982 *Phys. Lett.* A **90** 242
[80] Tahir N A and Long K A 1983 *Nucl. Fusion* **23** 887
[81] Tahir N A and Long K A 1984 *Laser Part. Beams* **2** 371
[82] Long K A and Tahir N A 1982 *Phys. Lett.* A **91** 451
[83] Long K A and Tahir N A 1986 *Nucl. Fusion* **26** 555
[84] Long K A and Tahir N A 1987 *Phys. Rev.* A **35** 2631
[85] Piriz A R 1988 *Phys. Fluids* **31** 658
[86] Piriz A R 1996 *Nucl. Fusion* **36** 1395
[87] Deutsch C 1986 *Ann. Phys. Paris* **11** 1
[88] Logan B G, Perkins L J and Barnard J J 2008 *Phys. Plasmas* **15** 072701